Warehouse Commodity Classification from Fundamental Principles. Part II: Flame Heights and Flame Spread

K.J. Overholt[a,*], M.J. Gollner[b], J. Perricone[c], A.S. Rangwala[a], F.A. Williams[b]

[a] *Worcester Polytechnic Institute, Department of Fire Protection Engineering. 100 Institute Road, Worcester, MA 01609-2280*
[b] *University of California, San Diego, Dept. of Mechanical and Aerospace Engineering. 9500 Gilman Drive, La Jolla, CA 92093-0411.*
[c] *Creative FPE Solutions, Inc., 1242 Thomas Avenue, San Diego, CA 92109*

Abstract

In warehouse storage applications, it is important to classify the burning behavior of commodities and rank them according to their material flammability for early fire detection and suppression operations. In this study, a preliminary approach towards commodity classification is presented that models the early stage of large-scale warehouse fires by decoupling the problem into separate processes of heat and mass transfer. Two existing nondimensional parameters are used to represent the physical phenomena at the large-scale: a mass transfer number that directly incorporates the material properties of a fuel, and the soot yield of the fuel that controls the radiation observed in the large-scale. To facilitate modeling, a mass transfer number (or B-number) was experimentally obtained using mass-loss (burning rate) measurements from bench-scale tests, following from a procedure that was developed in Part I of this paper.

Two fuels are considered: corrugated cardboard and polystyrene. Corrugated cardboard provides a source of flaming combustion in a warehouse and is usually the first item to ignite and sustain flame spread. Polystyrene is typically used as the most hazardous product in large-scale fire testing. The nondimensional mass transfer number was then used to model in-rack flame heights on $6.1 - 9.1$ m $(20 - 30$ ft) stacks of 'C' flute corrugated cardboard

*Corresponding author
Email address: koverholt@gmail.com (K.J. Overholt)

boxes on rack-storage during the initial period of flame spread (involving flame spread over the corrugated cardboard face only). Good agreement was observed between the model and large-scale experiments during the initial stages of fire growth, and a comparison to previous correlations for in-rack flame heights is included.

Keywords:
upward flame spread, flame height, commodity classification, B number, Group A plastic, warehouse fire

---

Nomenclature

Symbols

A_l	Eq. 10a
A_t	Eq. 10b
B	B-number / Spalding Mass Transfer Number, Eq. (2) $(-)$
c_p	Specific heat $(J/g\text{-}K)$
D	Species diffusivity (m^2/s)
d	Panel separation distance (m)
Gr	Grashof number $(-)$
ΔH_c	Heat of combustion (J/g)
ΔH_g	Heat of gasification (J/g)
g	Acceleration due to gravity (m/s^2)
h	Heat transfer coefficient $(W/m^2\text{-}K)$
h_c	Convective heat transfer coefficient $(W/m^2\text{-}K)$
h_r	Radiant heat transfer coefficient $(W/m^2\text{-}K)$
k	Thermal conductivity $(W/m\text{-}K)$
$\dot{m}''$	Mass-loss rate per unit area $(g/m^2\text{-}s)$
Nu	Nusselt number $(-)$
Pr	Prandtl number $(-)$
Q	Energy losses at fuel surface (W)
$\dot{q}_A''$	Volumetric heat release rate (kW/m^3)
$\dot{q}_c''$	Convective heat flux per unit area (kW/m^2)
$\dot{q}_{loss}''$	Surface heat loss rate (kW/m^2)
$\dot{q}_r''$	Radiant heat flux per unit area (kW/m^2)
$\dot{q}''(x)$	Surface heat flux per unit area (kW/m^2)
$\dot{q}''(0)$	Surface heat flux at pyrolysis height (kW/m^2)
$\dot{q}_F'$	Rate of forward heat transfer per unit width (W/m)
$\dot{q}_c'$	Rate of heat release by combustion per unit width (W/m)
r	Mass consumption number $(Y_{O,\infty}/\nu_s)$
T_f	Flame temperature (K)
T_m	Average temperature between flame and fuel surface (K)
T_p	Fuel pyrolysis temperature (K)
T_∞	Ambient temperature (K)
v_s	Stoichiometric oxygen-mass fuel ratio $(-)$
U	Free stream velocity (K)
V_{xp}	Velocity of pyrolysis front (m/s)
w	Panel/sample width (m)

x_f	Flame height (m)
x_p	Pyrolysis height (m)
Y_{O_2}	Mass fraction of oxygen (g/g)
Y_g	Soot yield of combustion gases (g/g)
Y_s	Soot yield of fuel (g/g)

Greek Symbols

α	Thermal diffusivity (m^2/s)
β	Thermal expansion coefficient $(1/K)$
χ	Fraction of flame radiation lost to the environment $(-)$
δ	Preheat distance (m)
ϵ	Emissivity $(-)$
ρ	Density (g/m^3)
μ	Viscosity $(kg/m\text{-}s)$
ν	Kinematic viscosity (m^2/s)
Φ	Forward heating parameter $(\Phi = \dot{q}'_F/\dot{q}'_c)$
σ	Stefan-Boltzmann Constant $(W/m^2\text{-}K^4)$
τ	Shear stress at surface (Pa)
ς_f	Nondimensional flame height $(-)$
ς_p	Nondimensional panel height $(-)$

Subscripts

F	Fuel
f	Flame
g	Gas
m	Mean
s	Solid
∞	Ambient

1. Introduction

Warehouse storage occupancies are currently reaching heights on the order of 24 to 30 m (80 to 100 ft) high stacks of storage commodity, which have not been considered by existing fire codes and engineering correlations. Over the last 50 years, fire protection engineers have relied on large-scale tests to classify commodities into one of seven classes [1] that are representative of their fire performance under specific geometric configurations and ignition conditions. This classification process, which relies on expensive full-scale testing, results in increased safety gaps as the industry creates new and untested materials that are stored in large quantities. Only a limited amount of fundamental science has been performed in this area, which is largely due to the range of complexities that occur in large-scale fire phenomena. Some correlations for large-scale flame heights of some commodities and fuels are present in the literature, but they are limited to specific fuels/configurations and some of the correlations require heat release rate values from full-scale tests. These correlations will be discussed further in the following sections of this paper. Currently, no tests that are known to the authors provide a complete set of fundamental, nondimensional parameters that can be used in engineering calculations towards the safer design of large storage facilities. Efforts that result in the development of such test methods and classification methodology with a sound scientific basis may fulfill an urgent need to improve upon the current warehouse design methods.

The motivation for this study was a series of recent losses in large warehouse storage facilities. In most of these incidents, which were reviewed in Part I of this paper, the facilities were protected by automatic sprinkler systems that were installed in accordance with their respective current codes and standards [2]. The negative impacts of these devastating fire incidents were felt by the occupants, firefighters, insurance interests, and local environments. From a business aspect, millions of dollars of materials or products are lost, and operations may be halted [3]. Furthermore, insurance premiums are increased as a result of the fire, and the lost time can never be recovered. From a life-safety aspect, the lives of workers and responding firefighters are endangered, which can result in injuries or death. The water runoff from firefighting operations and the resulting smoke plumes can also adversely affect the surrounding environment. The development of an approach to protect these facilities based upon the combustible materials that are stored, the layout of these materials, and the complex interaction with potential

suppression systems is a critical step towards reducing the amount of devastating warehouse losses. As a first step towards improving the methods for commodity classification, two existing nondimensional parameters are used to represent the physical phenomena present at the large-scale and model one part of large-scale flame spread.

In Part I of this paper, a method was developed to experimentally quantify the burning rate of a material based upon the nondimensional comparison of a materials chemical energy released during the combustion process with the energy required to vaporize the fuel, which was measured as a B-number. Commodities are classified to design sprinkler protection systems for most warehouse scenarios, and because such a sprinkler systems goal is to suppress or control a fire, the ranking of materials based upon the burning and spread rates of a potential fire is appropriate. Experiments were performed on a standard warehouse commodity, a Group A plastic, which is typically used to represent the worst-case commodity in large-scale tests. The commodity consisted of a single corrugated cardboard box that measured 53 x 53 x 51 cm and contained 125 crystallized polystyrene cups that were segregated by corrugated cardboard dividers. All of the faces except for the front face of the commodity were uniformly insulated, and the front face of the commodity was ignited at its base.

The experimental observations of the Group A plastic commodity resulted in a qualitative description of the burning process over three distinct stages of burning. The first stage was characterized by upward flame spread over the front face of the corrugated cardboard, followed by a decreased burning rate as the cardboard smoldered and the polystyrene heated, and finally a sharp increase in the burning rate after ignition of the polystyrene. Despite the complex configuration, each stage resulted in distinct material involvement, which indicates the potential to model distinct material involvement from each stage using parameters derived from bench-scale testing. Fluctuations between the repeated tests also indicated the difficulty in obtaining repeatable measurements during these larger tests; therefore, small-scale test methods that can be repeated at a level of statistical accuracy may greatly improve the applicability of the results.

Part II of this study continues the development of a nondimensional approach to characterizing the burning behavior of materials. The bench-scale tests that were performed in this study involved a small, flat sample (5 x 20 cm) of corrugated cardboard or polystyrene oriented vertically in which the burning was isolated to the front surface of the sample. The flow

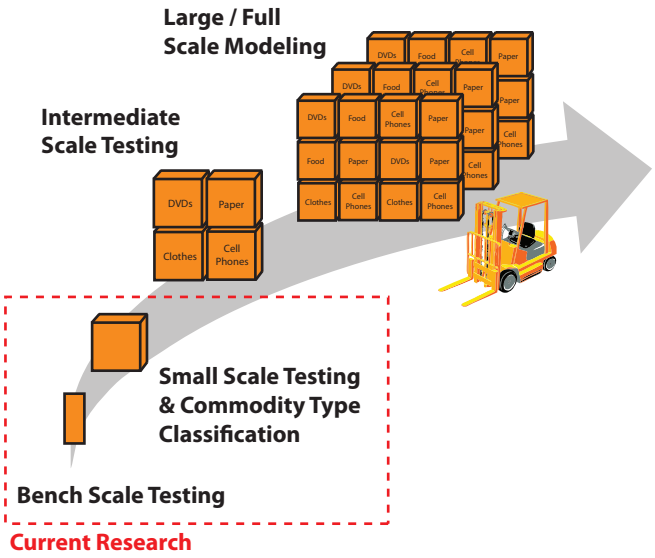

Figure 1: *A research approach to the warehouse fire problem. The two smaller scales studied in this work are shown by the dashed box.*

was considered to be laminar due to the observed behavior of the flow in the experiments. At the bench scale, the tests captured the effects of the commodity material properties on the flame spread process while separating the large-scale effects such as turbulence and radiation. Nondimensional B-numbers were experimentally determined for the samples with greater accuracy than previous experiments. A flame spread model was then utilized to demonstrate the application of the experimentally measured B-numbers to predict in-rack flame heights in large-scale configurations. A particular configuration considered in this study is upward flame spread in the flue space between corrugated cardboard, which is typical of warehouse storage arrangements. The model was extended to account for both convective and radiative heat transfer by incorporating convective and radiative heat transfer correlations. This segregated approach effectively uses a nondimensional parameter to represent the mass transfer processes, the gas phase heat transfer by including an appropriate convective heat transfer correlation, and radiative heat transfer effects that are based on previous studies.

2. Literature Review

Previous studies have attempted to model some of the large-scale effects of warehouse fires by measuring the relevant parameters using bench-scale test methods. One such effort by Hamins and McGrattan [4] constructed single-cell replicates of a Group A plastic commodity. The purpose of the Group A plastic tests was to provide input parameters into a computational fluid dynamics model using a measured heat release rate as the thermal loading input for a large-scale warehouse fire. The model predictions were unable to describe the detailed fire growth in storage applications.

Several studies have addressed the issue of upward flame spread on corrugated cardboard surfaces. Grant and Drysdale [5] modeled the flame spread along corrugated cardboard during the early growth stages of a warehouse fire by adapting the linearized Satio, Quintiere, and Williams [6] flame spread model with Karlsson's [7] burnout length and solving numerically. Dimensional parameters that were obtained experimentally were used as inputs to numerically model the flame height, velocity of the flame front, and pyrolysis front progression as a two-dimensional problem. Good agreement between the experimental results and the numerical results were obtained, although the model was found to be sensitive to averaged input parameters, such as the forward heat flux from the flame. Alvares et al. [8] studied the effects of panel separation on vertical flame spread and mass-loss rates in small-scale corrugated cardboard tests to determine the rate of fire growth along vertical flues in warehouses.

Continued efforts by Ingason and de Ris [9] and Ingason [10] have identified the importance of the commodity configuration, the mode of heat transfer, and the flue spacing of commodity boxes in warehouse fires. Ingason's work [9] identified some of the dominant factors in the large-scale warehouse fire growth process, and emphasized the importance of separating the material properties of the fuel from the heat transfer and flow conditions that can result due to the various configurations of the fuel packages. Experimental correlations of rack-storage fires are available in previous literature, including heat release rates [10–14], boxed in-rack flame heights [9, 10], in-rack plume temperatures [10], and heat fluxes [9, 15].

In separating the warehouse fire problem into two distinct phenomena, it then becomes a problem of defining the material properties (pyrolysis), flow conditions (geometry), and heat transfer (gas phase). Work performed by de Ris and Orloff [15], de Ris et al. [16], Foley [17], and Foley and Drysdale [18]

served to characterize the mode of heat transfer from an upward propagating flame in a warehouse configuration and to quantify the convective and radiative heat transfer that drives the upward flame spread process in the gas phase. Variations in the heat transfer from the small-scale to the large-scale was shown by de Ris et al. [16] to be related by similarity effects that are present in buoyant, turbulent boundary layer flows. This result can be used to extend the analytical results that were developed for heat and mass transfer in laminar boundary layers to turbulent boundary layers.

In the early stages of a warehouse fire, before the fire sprinklers are activated, the mass transfer is intrinsically coupled to the material properties of the stored commodity, packing material, and outer corrugated cardboard covering. Due to the different burning behavior of each material, which is also a function of the packing and orientation, the problem of classifying a commodity based on its fire hazard is a complex one. A general approach for describing the heat, mass, and momentum transfer by way of differential equations for simple geometries such as a droplet, flat horizontal, and vertical plate are discussed extensively in previous fire literature [19–22]. Physically, all of these theories rely on the extended Reynolds analogy that includes the combustion of solid fuels [23] in the form

$$\frac{\tau}{U\nu^{2/3}} = \frac{h}{c_p\alpha^{2/3}} = \frac{\dot{m}''}{D^{2/3}\ln(1+B)}. \tag{1}$$

Equation 1 is also referred to as the Chilton-Colburn [24] extension to the Reynolds analogy because it incorporates both of the turbulent and laminar molecular processes of diffusion by using the kinematic viscosity or momentum diffusivity (ν), the thermal diffusivity (α), and the species diffusivity (D). Equation 1 implies that the shear stress at the surface (τ) is related to the heat transfer (h/c_p) and mass transfer from combustion ($\dot{m}''$). The terms U, h, and c_p are the free stream velocity, heat transfer coefficient, and specific heat of the gas, respectively. The term B that appears in Eq. 1 is a nondimensional proportionality constant that relates the rate of mass transfer (e.g., vaporization, combustion) to the heat transfer and shear stress, which is referred to as the B-number in this work. A study by Raghavan et al. [25] further analyzed this proportionality and showed that Eq. 1 is valid except during the ignition and extinction conditions. Because the B-number in Eq. 1 represents the driving force for mass transfer, it is also referred as the "transfer number" by Spalding [26] and can be represented as the ratio

$$B = \frac{(1-\chi)Y_{O_2,\infty}(\Delta H_c/r) - c_p(T_p - T_\infty)}{\Delta H_g + Q}, \tag{2}$$

where χ is the fraction of radiation lost to the environment, $Y_{O_2,\infty}$ is the mass fraction of oxygen in the air, ΔH_c is the heat of combustion, r is the mass consumption number given by $(Y_{O,\infty}/v_s)$, c_p is the specific heat of air, T_p is the vaporization temperature of the fuel, T_∞ is the ambient temperature, ΔH_g is the heat of gasification, and Q represents the energy losses at the fuel surface [27].

The B-number is composed of material-related properties; therefore, it has been used to describe the flammability of materials in previous fire literature [28–31]. A problem that often remained in the past studies was implementing the B-number to assess large-scale behavior, which will be further discussed in this study. Figure 2 shows the B-numbers for a range of fuels [30] as a function of the pyrolysis temperature of the materials. The points indicate the values of the thermodynamic B-number versus the pyrolysis temperatures for the fuels as calculated by Annamalai and Sibulkin [30]. In the past, thermodynamic values of B-numbers have been calculated using Eq. 2 where χ and Q are assumed to be equal to zero, which represents an ideal value with no losses. The liquid fuels shown in Fig. 2 have a larger B-number value and a lower pyrolysis temperature, which corresponds to a smaller amount of energy required to gasify liquid fuels versus solid fuels. The value for α-cellulose shown in the figure is an ideal value that does not incorporate any losses, which results in a dramatic shift in its B-number value. In general, a lower B-number indicates a higher pyrolysis temperature because the fuel requires more energy to gasify. Therefore, a larger B-number indicates a fuel that has a higher thermodynamic efficiency during combustion [32].

A simple description of mass transfer is derived by rearranging Eq. 1 for the mass-loss rate to yield the expression

$$\dot{m}''_f = \frac{\overline{h}}{c_p} \ln(1+B) \tag{3}$$

with the assumption of a unity Lewis number in which the thermal and mass diffusivities are assumed to be equal. Equation 3 will be used to determine a B-number for a given fuel by experimentally measuring the mass-loss rate.

As explained in a recent publication [33], a number of improved laminar boundary layer types of theories result in formulas that are more complicated

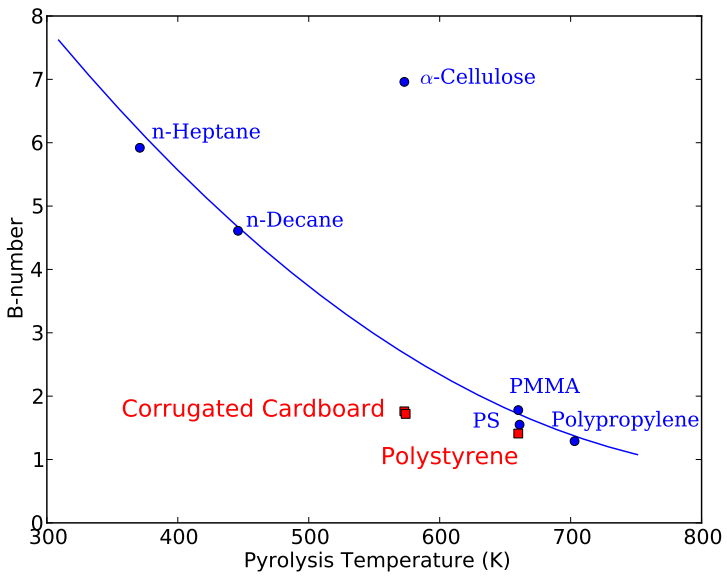

Figure 2: *Values of the B-number for a range of fuels. The points are B-number values from Annamalai and Sibulkin [30] that were calculated using only the thermodynamic properties. The red squares indicate the B-number values that were obtained experimentally in this study.*

than Eq. 3, but the results are qualitatively the same. In larger tests that were previously performed, the fluctuating flames and the incipient turbulence raise questions about the degree of applicability of such theorems. For these reasons, this simple description of the mass transfer, Eq. 3, was chosen in this study over other relevant expressions.

In this study, the B-number is primarily a function of the material properties of a given fuel and it is obtained in a controlled experimental environment by assuming that the primary mode of heat transfer at the bench-scale is convection [34]. This assumption is reasonable for the small, laminar flames observed in this study. In examining Eq. 2, the B-number can be considered to be a ratio of the available energy (heat of combustion) to the energy required to gasify a given fuel (heat of gasification). Thus, the B-number is intrinsic to the properties of a material and is therefore independent of a particular scale. This allows for the results from the bench-scale tests to be used as a material input (instead of the heat release rate) for the prediction of large-scale warehouse fire behavior.

3. Experimental Setup and Procedure

Figure 3 shows a schematic of the experimental setup. A total of 9 tests were conducted using two different samples: single-wall corrugated cardboard (6 tests) and polystyrene (3 tests). The samples measured 5 cm wide by 20 cm in height. This aspect ratio was selected because laminar flames were the primary focus of the bench-scale tests due to the more controllable environment for isolating material properties and separating gas-phase phenomena, and upwardly-spreading flames typically become turbulent above 20 cm [35], which is accounted for in a later section when large-scale warehouse fires are considered. For the bench-scale tests, a transition to a turbulent regime was not considered for simplicity, which agreed with visual observations. For this study, the sample width was fixed at 5 cm to minimize the amount of variance between the tests and because a smaller sample size may affect the amount of combustible gases generated by the fuel due to significant diffusion of the fuel to the sides of the sample [36].

The typical mass of the samples was 4 g for corrugated cardboard and 36 g for polystyrene. Corrugated cardboard and polystyrene were chosen to be tested because they are the components of a Group A plastic commodity that is used to represent a worst-case fire scenario in large-scale warehouse tests. Additionally, corrugated cardboard is typically the first item to ignite

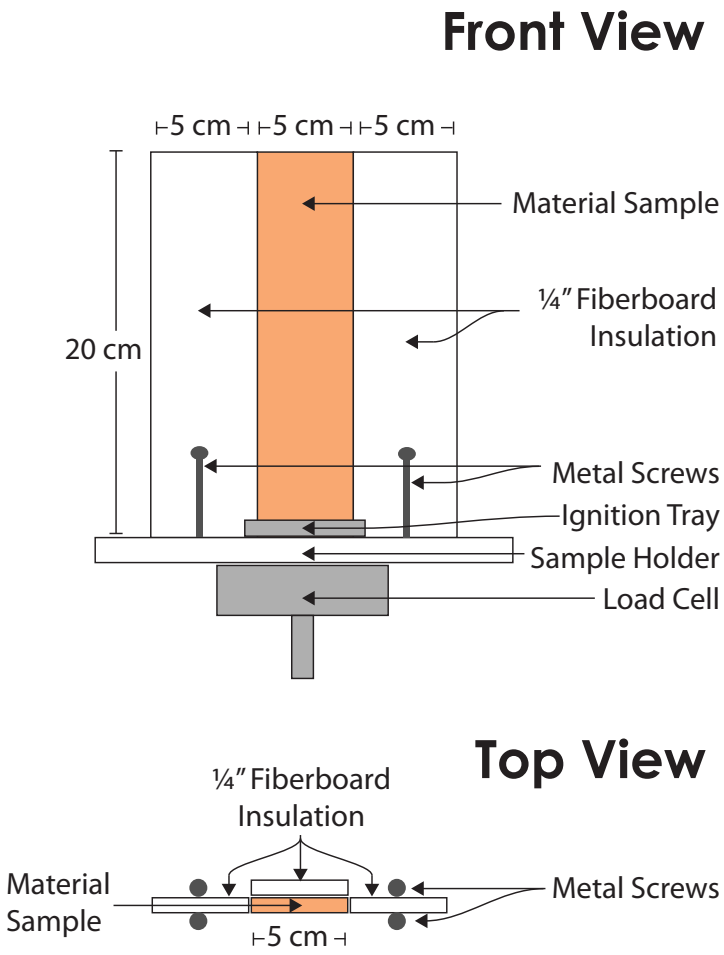

Figure 3: *Schematic of the experimental setup.*

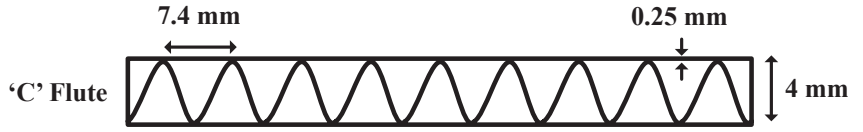

(a) Corrugated cardboard

(b) Polystyrene

Figure 4: *Cross-sectional detail of the samples that were used in the tests: (a) Corrugated cardboard, 4-mm thick. The paper sheets are of a 100 g (26-26-26 lb) basis weight. (b) Polystyrene sheets, 3-mm thick.*

and sustain flame spread in a warehouse fire. The measured quantities for each test included the mass-loss rate, flame height, and pyrolysis height.

The corrugated cardboard used in these tests was identical to the configuration and thickness that is used to package standard Group A plastics, and of the same type used in the small-scale tests that were performed by the authors in Part I [2]. The corrugated cardboard samples were of a type 'C' flute with a nominal thickness of 4 mm and 135 flutes per meter width [37] as shown in Figure 4(a). All of the tests were performed with the flutes aligned vertically along the 20 cm dimension, which is similar to the orientation of the flutes in an upright commodity box. The polystyrene samples were 3 mm thick as shown in Figure 4(b).

The mode of ignition for the tests was a small aluminum tray measuring 5 x 0.5 x 0.5 cm (Figure 3) that was placed at the base of the sample and contained a thin strip of glass fiber insulation soaked with n-heptane. This ensured a uniform mode of flaming ignition along the base of the fuel sample. The corrugated cardboard tests used 0.25 mL of n-heptane for ignition, whereas the polystyrene tests used 0.75 mL of n-heptane because it took a longer time for the polystyrene samples to ignite. After initial ignition of the n-heptane, the n-heptane typically burned out within 5-10 seconds and only served to ignite the fuel sample uniformly along the bottom edge.

All of the fuel samples were insulated on the back and sides with 0.64 mm (0.25 inch) thick fiberboard insulation to isolate the burning to the front face of the samples only. The samples were secured in place by the insulating

fiberboard sheets that were supported by four metal screws attached to the 1.9 cm (0.75 inch) thick fiberboard base (Figure 3). All of the corrugated cardboard tests burned to completion and self-extinguished once the fuel was depleted. The polystyrene samples were manually extinguished after the flame reached a pyrolysis height of about 10 cm due to excessive smoke production and dripping on the bench-scale apparatus. However, the dripping and deformation of the polystyrene was not considered to be significant during the time frame considered in the results because the sample size in the experiment was small, and a significant accumulation of melted polystyrene was not observed during this time period.

The mass lost by the specimen was measured continuously using a load cell (Automatic Timing & Controls model 6005D) with an accuracy of $\pm$ 0.5 g as specified by the manufacturer. This is approximately 12% of the nominal initial mass of the corrugated cardboard samples and 2% of the nominal initial mass of the polystyrene samples. The load cell was calibrated prior to each test series using standard test weights. To measure the flame heights and record the burning history of the tests, video and still images were captured using a Sony Handycam HRR-SR5 model camera and a Canon EOS-5D digital single-lens reflex (DSLR) camera. Figure 5 depicts a visual time history of the vertical flame spread along a corrugated cardboard sample. The images were then loaded onto a computer, and a MATLAB image processing script was used to visually determine the flame heights as a function of time from each test. The flame height was defined as the tip of an attached yellow flame and was selected visually (by selecting the flame tip with the mouse pointer) from each picture by using the script. The processed images and resulting flame heights were consistent with visual comparisons from the test videos.

Similar to the flame heights, observations of the visual charring on the corrugated cardboard was used to determine the location of the pyrolysis front. For the polystyrene samples, visual bubbling and charring from the video were used to determine the location of the pyrolysis front. The corrugated cardboard and polystyrene tests were fairly repeatable, and the heights of the pyrolysis front in the laminar regime were fairly similar; thus, a best-fit functional approximation of the pyrolysis heights was made. This approximation was later used to determine an average mass-loss rate per unit area ($\dot{m}''_f$), and finally, a B-number was calculated for each test. After the maximum pyrolysis height was reached, a constant height of 20 cm (for the corrugated cardboard) or 10 cm (for the polystyrene) was assumed, which represents the

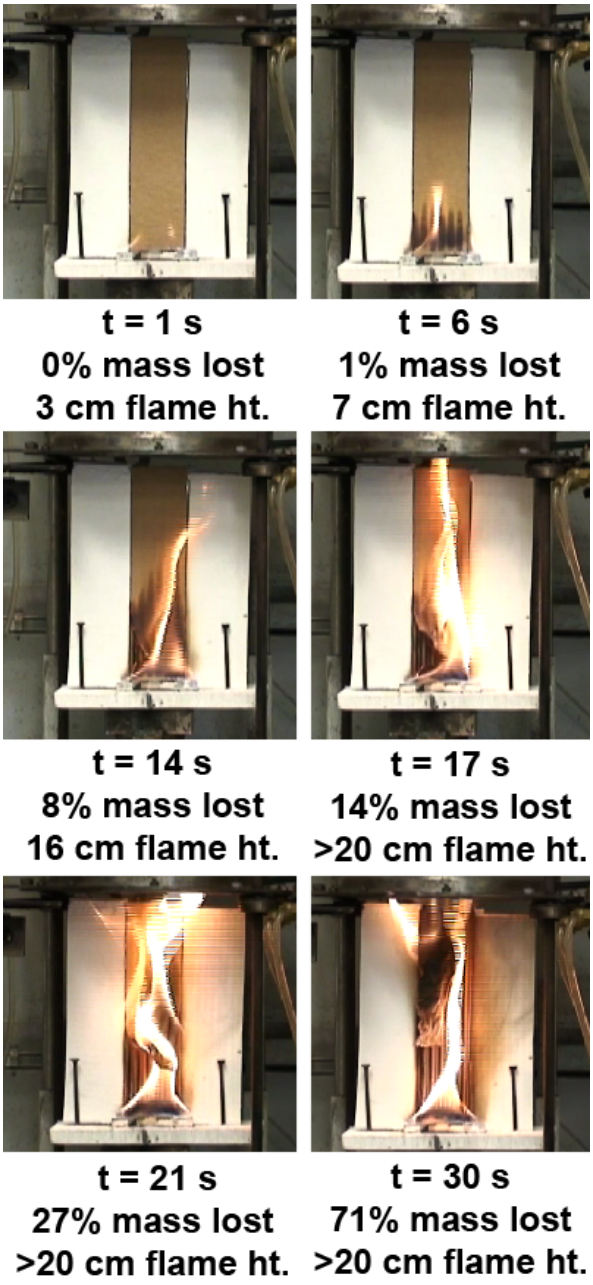

Figure 5: *Snapshots from a bench-scale test with a corrugated cardboard sample. Each picture shows the current time, percent of total mass lost, and flame height.*

entire surface of the front face of the sample.

4. Experimental Results and Discussion

The results described in this section are based on a total of 9 bench-scale tests that were performed using the two samples that were discussed in Section 3. After ignition along the base of the samples, the flame spread in the upward direction along the fuel samples. Due to edge effects along the fuel sample, a small amount of two-dimensional flame spread (both vertically and horizontally) occurred in the experiment. As the excess pyrolyzate burned above the pyrolysis zone, the unburned fuel above the pyrolysis zone (x_p) was heated to its ignition temperature and the flame spread in the upward direction at an increasing rate [38]. As described in Section 3, the mass-loss rates were trimmed to the time period during upward flame spread along the samples.

During the period of upward flame spread, the average value of $\dot{m}''_f$ for corrugated cardboard was within a range of $7.3 - 7.9 \cdot 10^{-4}$ g/cm^2-s, and for polystyrene was within a range of $6.7 - 6.8 \cdot 10^{-4}$ g/cm^2-s. Figures 6(a) & 6(b) show the flame heights that were measured in the bench-scale experiments for corrugated cardboard and polystyrene and the least-squares fit to the pyrolysis height that was used to determine the area burning, and later the average B-numbers for the corrugated cardboard and polystyrene samples. Using an average value from all of the tests that were performed on a given material sample, the B-number for corrugated cardboard was calculated to be 1.7 (standard deviation of 0.08) and for polystyrene was calculated as 1.4 (standard deviation of 0.02). The B-numbers were then used in the flame spread model as described in Section 5 to predict the flame heights for both the bench-scale and large-scale cases.

The mass-loss rate data were trimmed to contain only the time period where upward flame spread occurred along the sample, removing data prior to ignition of the sample and after the pyrolysis front has reached the top of the sample. By reviewing the video recordings and mass-loss data for a particular test, Figure 7 shows the period after ignition and the omitted period after the flame reached the top of the sample. The trimmed (shaded) portion of the data was used to determine an average $\dot{m}''_f$. After the mass-loss rate was trimmed, it was then fit with a 4th-order polynomial to obtain a smooth mass-loss curve; the 4th order fits exhibited at least a 99% R^2 value for each of the mass-loss data sets. The mass-loss data were then divided by

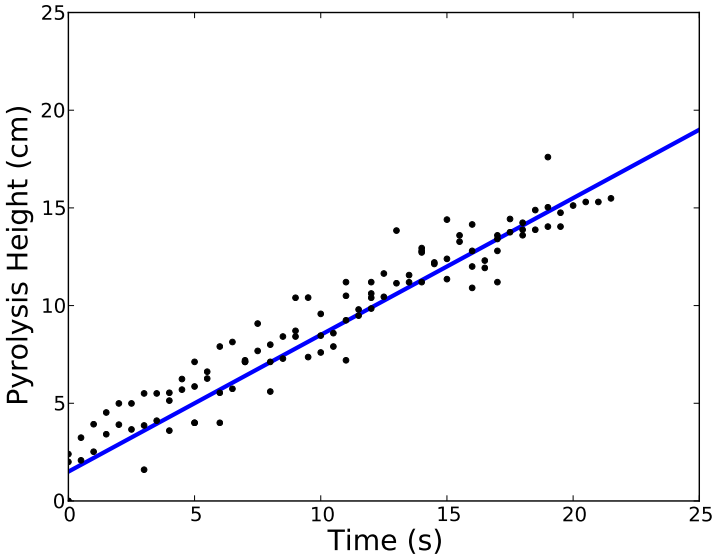

(a) Corrugated cardboard

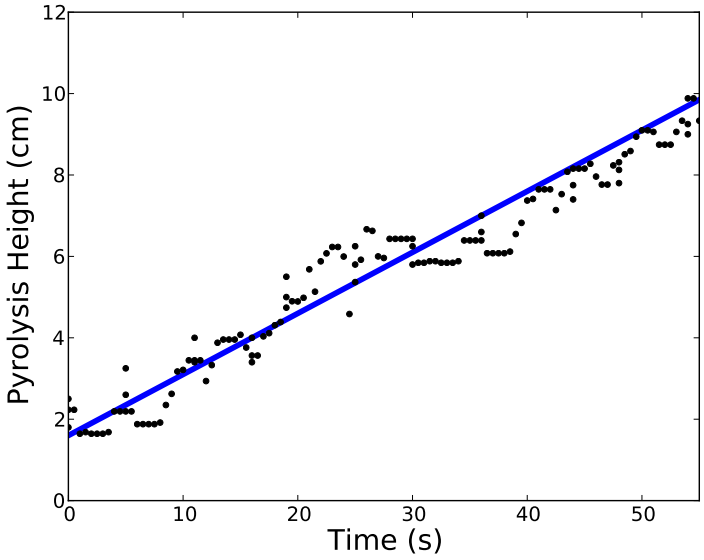

(b) Polystyrene

Figure 6: *Pyrolysis heights observed in the bench-scale tests. The points indicate the observed pyrolysis heights, and the solid lines indicate linear fits for the pyrolysis height data, which were used to calculate the burning area.*

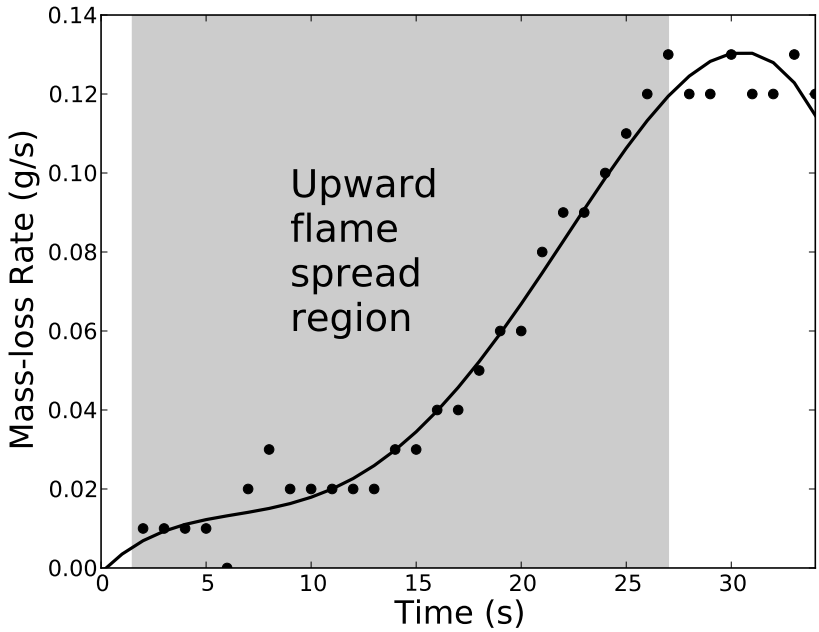

Figure 7: *Mass-loss rate for a representative corrugated cardboard test. The points indicate the mass-loss data from the load cell, and the solid line shows the 4th-order polynomial fit used to calculate the mass-loss rate used in the B-number calculation. The shaded region shows the trimmed portion of the mass-loss rate consisting solely of upward flame spread, where regions of ignition and burnout of the material have been removed.*

Table 2: *Average $\dot{m}''_f$ for each of the cardboard and polystyrene tests.*

Test	$\dot{m}''_f$ $(kg/m^2\text{-}s)$
Cardboard 1	7.7
Cardboard 2	7.8
Cardboard 3	7.4
Cardboard 4	7.5
Cardboard 5	7.9
Cardboard 6	7.3
Polystyrene 1	6.8
Polystyrene 2	6.7
Polystyrene 3	6.8

the pyrolysis height data fits and the width of the sample to obtain an average $\dot{m}''_f$ for each of the tests. The average $\dot{m}''_f$ values for each of the cardboard and polystyrene tests are shown in Table 2. Figure 8 shows the mass-loss rates for each of the corrugated cardboard and polystyrene tests. From the previous step, the mass-loss rates shown here were previously trimmed to the observed time that it took for the pyrolysis height to reach the top of the sample. In this figure, the initial time ($t = 0$) corresponds to the time at which the sample was ignited and could sustain a flame without the pilot flame present. During this initial ignition period (typically less than a few seconds), some gasification occurred but was not sufficient to sustain the combustion of the material, which is the reason that some of the mass-loss rate fits exhibit a mass-loss rate slightly above zero at $t = 0$.

The value of $\dot{m}''_f$ was then put into the experimental B-number formulation given by

$$B = \left(\frac{\dot{m}''_f}{\rho_g \alpha_g 0.59 / x_p [g x_p \beta \Delta T / \alpha_g \nu_g]^{1/4}} \right) - 1, \tag{4}$$

which uses a correlation for natural, laminar convection along a vertical plate, $Nu = 0.59(GrPr)^{1/4}$ [37], $\dot{m}''_f$ is the average mass-loss rate, ρ_g is the density of air, α_g is the thermal diffusivity of air, x_p is the pyrolysis height, g is the acceleration due to gravity, β is the thermal expansion coefficient given by $1/T_m$, $\Delta T = T_m - T_\infty$, and ν_g is the kinematic viscosity of air. For the flame temperature, a typical turbulent average flame temperature was used in the calculations as $T_f = 800°\text{C}$ [39]. An equation similar to Eq. 4 for turbulent

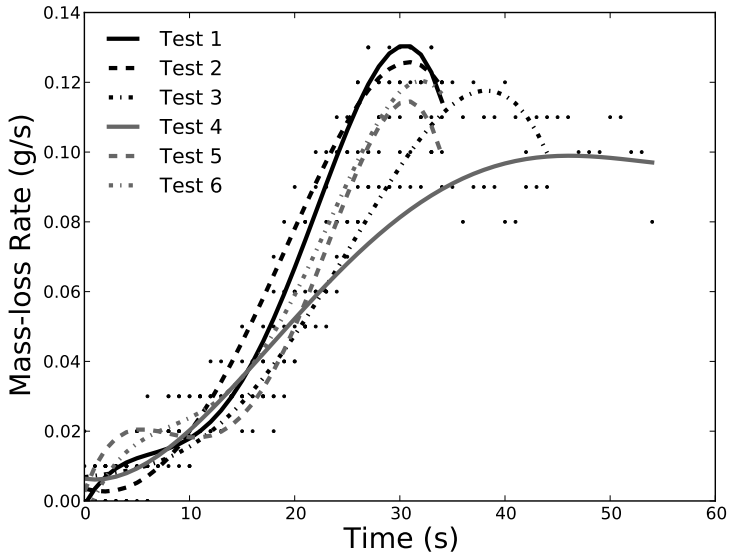

(a) Corrugated cardboard

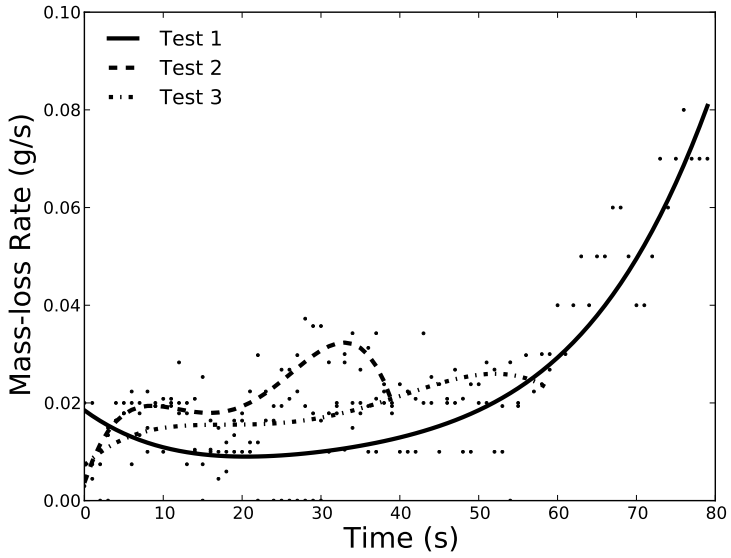

(b) Polystyrene

Figure 8: *Mass-loss rate vs. time for the corrugated cardboard and polystyrene test samples. The points indicate the measured mass-loss rates, and the lines indicate the polynomial fits for the mass-loss rates, which were used to calculate the B-number.*

Table 3: *Gas-phase properties used to calculate the B-number (Eq. 4) estimated at a mean temperature of 683 K [41].*

Property	Value
ρ_g	$0.50\ kg/m^3$
α_g	$98 \cdot 10^{-6}\ m^2/s$
Pr	0.7
T_m	$683\ K$
T_∞	$298\ K$

flow is derived fully in Part I of this paper [2]. Table 3 lists all of the values used in Eq. 4. The thermo-physical properties of air are estimated at a mean gas temperature (T_m) and are assumed to be constant [40].

5. Flame Spread Model

Figure 9 shows a schematic of the upward flame spread model from Sibulkin and Kim [42] that was used to predict the flame heights as a function of the B-number. The pyrolysis zone is defined as the region of the solid fuel up to the pyrolysis height (x_p) where combustible fuel vapors are outgassing. Some of the fuel burns directly in front of the combusting fuel surface, while some of the fuel is carried by buoyancy above its height of origin and burns above, which heats the virgin material in the preheat zone ($\delta = x_f - x_p$) up to its ignition temperature. The fuel carried above the pyrolysis zone has been called *excess pyrolyzate* [38] and forms the physical flame height (x_f) in which the resulting heat output drives the flame spread process. The rate of upward flame spread depends both on the amount of energy released by the combusting fuel and the rate at which the material pyrolyzes due to the flame heat flux, $\dot{q}''(x)$. This energy feedback from the gas phase to the condensed phase is the driving mechanism for the flame spread process. The B-number describes this feedback process as a nondimensional ratio.

The analytical model from Sibulkin and Kim [42] was adapted and solved numerically by using heat flux profiles from previous correlations. The heat flux is assumed to be constant along the pyrolysis region up to the pyrolysis height, and the flame spread occurs in one-dimension (vertically) along the sample. In the preheat region (δ), the heat flux decays exponentially as a function of distance (x), which follows from the heat flux distribution mea-

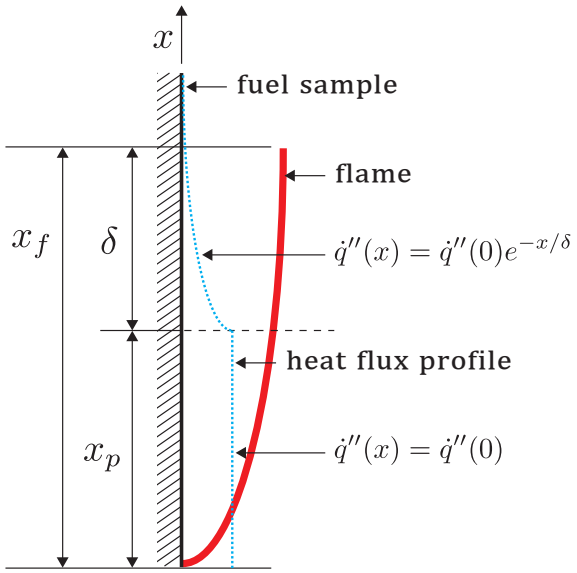

Figure 9: *The upward flame spread model proposed by Sibulkin and Kim [42]. x_p is the pyrolysis height, x_f is the flame height, δ is the preheat distance, and $\dot{q}''(x)$ is the flame heat flux (dotted line).*

surements by Sibulkin and Lee [43]. This heat flux condition is detailed in Eqs. 5a & 5b. Once the material in the preheat region reaches its pyrolysis temperature, it begins to outgas combustible vapors and the pyrolysis region grows, resulting in a larger flame height and more energy feedback to the unburned fuel; then the process repeats. Therefore, the process of upward flame spread can be thought of as a moving ignition front, similar to the leapfrogging process first described by de Ris [44].

Following from the concept of a moving ignition front, when solving the flame spread process numerically, the material sample is discretized into sections measuring 0.1 cm in height, and the initial conditions for the pyrolysis height and flame height that were observed in the experiments at the ignition time (t=0) are input into the model. The heat flux profile is mapped along the height of the sample (as in Figure 9) by applying the following boundary conditions at the surface

$$\dot{q}''(x) = \dot{q}''(0)\exp\left(-x/\delta\right) \quad \text{for } x > x_p \tag{5a}$$

$$\dot{q}''(x) = \dot{q}''(0) \quad \text{for } x \leq x_p \tag{5b}$$

Table 4: *Physical properties used in the flame spread model for corrugated cardboard and polystyrene*

Property	Corrugated Cardboard	Polystyrene	Units
k	0.06 [45]	0.12 [30]	$W/m\text{-}K$
ρ_s	115 [46]	1065 [30]	kg/m^3
c_p	1.20 [47]	1.34 [30]	$J/g\text{-}K$
ΔH_c	14,090 [48]	23,610 [48]	J/g
ΔH_g	2,200 [47]	1,590 [47]	J/g
T_p	573 [30]	660 [30]	K

where $\dot{q}''(0)$ is constant but can be modified to account for radiation from the flame, x is the height along the fuel sample, and δ is the preheat region. A Nusselt number correlation is used to describe the turbulent, convective heat transfer process that is present at the large scale. An appropriate correlation was used for natural, turbulent convection along a vertical plate, $Nu = 0.13(GrPr)^{1/3}$ [37]. Using this definition for the convective heat transfer coefficient, the initial heat flux, $\dot{q}''(0)$, to be used in Eqs. 5a & 5b can be approximated as

$$\dot{q}''(0) = \dot{q}''_c = \overline{h}_c(T_f - T_\infty), \tag{6}$$

which neglects radiant heat transfer, and where $\overline{h}_c$ is the convective heat transfer coefficient, T_f is the flame temperature for cellulosic materials ($T_f = 800°\text{C}$) [39, 40], and T_∞ is the ambient temperature. This results in a total heat flux from the flame, $\dot{q}''(0)$, of 5.2 kW/m^2 for this configuration. Heat fluxes that incorporate both convection and radiation will be later discussed when considering large-scale warehouse radiation effects, which essentially modifies the $\dot{q}''(0)$ term in Eqs. 5a & 5b.

After the heat flux is mapped along the height of the sample for the first time step, the forward heating parameter, ϕ, is calculated and later used to find the velocity of the pyrolysis front. The forward heating parameter (ϕ) was defined by Sibulkin and Kim [42] as the ratio of the forward heat transfer rate to the rate of heat release per unit width of the fuel ($\phi = \dot{q}'_F/\dot{q}'_c$). The forward heat transfer rate ($\dot{q}'_F$) is calculated by the integral of the heat flux

above the pyrolysis length (x_p) as in

$$\dot{q}'_F = \int_{x_p}^{\infty} \dot{q}''(x)dx, \tag{7}$$

where $\dot{q}''(x)$ is the heat flux along the height of the sample (Eq. 5a), and $\dot{q}'_c$ is the rate of heat release per unit width of the sample given by $\dot{q}'_c = \dot{m}'_f \Delta H_c$. An expression for the mass flux from the pyrolysis region ($\dot{m}'_f$) obtained by Sibulkin and Kim and used in their flame spread model [42] is given by

$$\dot{m}'_f(x_p) = 0.59 \frac{\mu_f}{Pr^{3/4}} \left(\frac{g\beta\Delta T}{\nu_g} \right)^{1/4} \ln(1+B) x_p^{3/4} \text{ (laminar)}, \tag{8a}$$

$$\dot{m}'_f(x_p) = 0.13 \frac{\mu_f}{Pr^{2/3}} \left(\frac{g\beta\Delta T}{\nu_g} \right)^{1/3} \ln(1+B) x_p^{3/4} \text{ (turbulent)}, \tag{8b}$$

where μ_f is the viscosity of air, Pr is the Prandtl number, g is the acceleration due to gravity, β is the thermal expansion coefficient, ΔT is defined as $(T_m - T_\infty)$, ν_g is the kinematic viscosity of air, B is the B-number for the material as calculated by Eq. 4, and x_p is the pyrolysis height. The flame spread model switches to the turbulent formulation if the flame height (x_f) becomes greater than 20 cm in length [35], which is later used when validating the model against large-scale fire test data. Once the forward heating parameter (ϕ) is calculated from $\phi = \dot{q}'_F / \dot{q}'_c$, the velocity of the moving pyrolysis front for the current time step is calculated by

$$V(x_p) = A_l \phi x_p^{1/2} \text{ (laminar)}, \tag{9a}$$

$$V(x_p) = A_t \phi x_p \text{ (turbulent)}, \tag{9b}$$

where the terms A_l and A_t are given in by Sibulkin and Kim [42] by

$$A_l = \frac{\Delta H_c \Delta H_g}{(4/3)\rho_s c_s k_s (T_p - T_\infty)^2} \left[0.59 \frac{\mu_f}{Pr^{3/4}} \left(\frac{g\beta_f \Delta T}{\nu_g^2} \right)^{1/4} \ln(1+B) \right]^2 \text{ (laminar)}, \tag{10a}$$

$$A_t = \frac{\Delta H_c \Delta H_g}{\rho_s c_s k_s (T_p - T_\infty)^2} \left[0.13 \frac{\mu_f}{Pr^{2/3}} \left(\frac{g\beta_f \Delta T}{\nu_g^2} \right)^{1/3} \ln(1+B) \right]^2 \text{ (turbulent)}, \tag{10b}$$

where ΔH_c is the heat of combustion, ΔH_g is the heat of gasification, ρ_s, c_s, and k_s are thermophysical properties of the solid fuel, T_p is the pyrolysis temperature of the solid fuel, and the remaining terms were defined in Eqs. 8a & 8b. Table 4 lists the material properties for corrugated cardboard and polystyrene that are used in Eqs. 10a & 10b.

The resulting change in the flame height (due to the upward velocity of the pyrolysis front) is added to the current pyrolysis height for the next time step as $x_p[t + \Delta t] = x_p[t] + V[t]dt$. In the final calculation of the time step, the pyrolysis height is converted to the height of the flame tip by using an expression by Annamalai and Sibulkin [29] for natural convection as given by

$$x_f = 0.64(r/B)^{-2/3} x_p. \tag{11}$$

where r is the mass consumption number given by $(Y_{O,\infty}/\nu_s)$, and B is the B-number for the material. The values of r were used as 0.194 for cardboard and 0.0749 for polystyrene [30]. This assumption of a constant ratio of the flame height to the pyrolysis height is based on the simplification that the burning rate is a function of the incident heat flux and that all of the excess fuel above the pyrolysis region is burned [29, 38]. After the new flame height (x_f) is calculated, the numerical routine continues to the next time step and the process repeats starting from Eqs. 5a & 5b. This results in the prediction of the flame height as a function of time, i.e., a flame spread prediction.

The primary driving force of upward flame spread is the heat flux from the advancing fire plume towards the unburned material [49]. In a warehouse setting, this heat transfer may manifest itself in the form of strong convective currents tunneled through flue spaces or as soot-induced radiation from large, luminous fire plumes. As a first approximation, the convective heat transfer was used from the standard engineering correlations for turbulent boundary layer flows (Eq. 6).

To predict flame heights in large-scale fires, both convection and radiation must be incorporated into the flame spread model, which effectively modifies the $\dot{q}''(0)$ term in Eqs. 5a & 5b. A simple method to incorporate radiation is to include a radiation heat transfer coefficient [50] in Eq. 6, which results in

$$\dot{q}''(0) = \dot{q}_c'' + \dot{q}_r'' = \overline{h}_c(T_f - T_\infty) + h_r(T_f - T_\infty), \tag{12a}$$

$$\text{where } h_r = \frac{\sigma(T_f^2 + T_\infty^2)(T_f + T_\infty)}{1/\epsilon_1 + (A_1/A_2)(1/\epsilon_2 - 1)}, \tag{12b}$$

$\dot{q}''_c$ is the convective heat flux, $\dot{q}''_r$ is the radiative heat flux, h_c is the convection heat transfer coefficient, h_r is the radiation heat transfer coefficient, σ is the Stefan-Boltzmann constant ($5.67 \cdot 10^{-8}$ W/m^2-K^4), ϵ is the emissivity of the flame (assumed to be unity), and A_1 and A_2 are the area of the source and the target, respectively, which are equal in the numerical model. This results in a total flame heat flux in which $\dot{q}''(0) = 80$ kW/m^2.

A modified method for representing the radiation in large-scale warehouse flues is to incorporate a radiant heat-flux correlation based on work by de Ris and Orloff [15] for radiant heat transfer between parallel panels. As previously mentioned, in this study, the flow and geometry effects were separated from the effects of the mass transfer. Therefore, this expression is useful for various geometries, including the geometry in a warehouse storage configuration, in which the flame spread can be considered to be occurring between two parallel plates represented by the flue space between the rows of stored commodities. Following the method of de Ris and Orloff [15], the radiant heat flux is calculated using

$$\dot{q}''_r = \left(\frac{\varsigma_p \dot{q}'''_A w^2 d}{2 x_f w} \right) + \dot{q}''_{loss}, \tag{13a}$$

$$\text{and } \varsigma_p = \frac{\beta_1 (Y_s + Y_g)^{1/4} \varsigma_f}{\varsigma_f + \alpha_p \varsigma_f + \alpha_p} - \frac{2 \beta_2 \dot{q}''_{loss}}{d \dot{q}'''_A} \tag{13b}$$

where ς_p is the nondimensional panel width, $\dot{q}'''_A$ is the volumetric heat release rate assumed to be 1110 kW/m^3 [15], w is the sample width, d is the separation distance of the panels, x_f is the flame height, $\dot{q}''_{loss}$ is the surface heat loss rate fixed at a constant value of 5 kW/m^2 [15], and β_1 and β_2 are constants equal to 1.04 and 1.7, respectively. Y_s is the soot yield of the fuel equal to 0.01 g/g for a low-sooting fuel such as corrugated cardboard, and Y_g is added to the soot yield to account for radiation from the combustion gases for fuels having little to no soot and is equal to 0.01 g/g [15]. ς_f is the nondimensional flame height equal to x_f/w, and α_p is the aspect ratio equal to d/w.

In this formulation for the radiant heat flux, an increase in the panel separation distance (d) results in an increased radiant heat flux because the space between the panels is assumed to be fully occupied by flames. Thus, the separation distance for this study was fixed at 0.15 m (6 inches), which is representative of the flue space that is present in a typical warehouse commodity fire test. This expression for the radiant heat flux is dependent on

both the flame height and the soot yield of the fuel, which are important factors to consider when modeling flame spread at the warehouse scale. In this study, a representative value for the soot yield (Y_s) was chosen as 0.01 g for a cellulosic material such as corrugated cardboard, which is a very low sooting fuel. The soot yields are assumed to be constant; however, by using more information on the smoke point of the fuel from the bench-scale experiments, a variable soot yield can also be implemented. Using the results from Eqs. 13a & 13b for the radiant heat flux, a final expression for the flame heat flux is given by

$$\dot{q}''(0) = \overline{h}_c(T_f - T_\infty) + \left(\frac{\varsigma_p \dot{q}'''_A w^2 d}{2x_f w}\right) + \dot{q}''_{loss}. \tag{14}$$

and results in a total flame heat flux in which $\dot{q}''(0) = 27\ kW/m^2$.

Quantifying the heat flux from the the flame to the fuel bed in complex geometries is a challenging yet important task that is required to further develop a quantitative description of warehouse fire behavior. Evaluating the radiative and convective heat flux fractions is not easily accomplished for a large assortment of practical geometries, but computational fluid dynamics software (CFD) allows for the possibility of modeling these complex flow conditions. If the pyrolysis rate of the fuels is effectively handled by the B-number in such CFD codes, then the other flow conditions may be more easily resolved, which highlights the potential applications of this work in the future.

6. Flame Spread Model Results and Discussion

The results from the flame spread model were compared to the bench-scale results by using the observed flame heights from the videos of each of the 9 tests. Figure 10(a) shows the flame heights for corrugated cardboard as predicted by the model versus the bench-scale flame heights from the experiments. The flame height predictions for corrugated cardboard are in good agreement with the experimental flame heights. Figure 10(b) shows the flame heights for polystyrene as predicted by the model versus the bench-scale flame heights from the experiments. The flame height predictions for polystyrene are in good agreement with the experimental flame heights at the bench-scale. The bench-scale predictions are in reasonable agreement with the experimental flame heights because the dominant mode of heat transfer in the tests was assumed to be laminar, natural convection on a vertical plate,

and the same mode of heat transfer is assumed in the flame spread model as shown in Eq. 6. The thermal behavior of the fuel samples was considered to be a slab of finite thickness, and a more detailed analysis can be found in Overholt [51].

The average B-number for corrugated cardboard (1.7) was used in the large-scale flame spread predictions because it is nondimensional and describes the mass flux for both the bench-scale and large-scale scenarios. Previous studies have shown that the B-number is not constant, but varies to some degree in both time and space. Spatial variation cannot be captured using the method discussed in this paper; however, a time-averaged B-number has been shown to be valid to predict flame heights [27]. For the purposes of the large-scale, in-rack flame height predictions, the B-number was assumed to have a constant value of 1.7.

The results from the flame spread model were then compared to the large-scale by using in-rack flame heights from the rack-storage warehouse fire tests. The in-rack flame heights for the large-scale warehouse fires were obtained from video data from three large-scale warehouse commodity fire tests that were performed at Underwriter's Laboratory in Northbrook, Illinois [52]. The fuel consisted of paper cups (Class III commodity) that were packed in corrugated cardboard boxes and stacked between 6.1 m to 9.1 m in height (20 and 30 ft) in a rack-storage configuration. The boxes were ignited along the bottom edge in the flue space between the racks. Figure 11 shows a snapshot from a warehouse fire test as the flame spreads up through the flue space between the boxes.

The flame spread model predictions for the in-rack flame heights were compared to experimental flame heights from the three large-scale UL tests described above, and the results are shown in Figure 12. The points on the graph indicate observations of experimental flame heights from three large-scale UL tests as extracted from the test videos. The spread in the flame height data may be caused by many factors including minor deviations in ignition and ambient conditions, especially the moisture content of the cardboard. The data still, however, present a representative range of realistic tests performed. The three dashed lines indicate the flame height predictions using the experimentally determined B-number for three different flame heat fluxes. To incorporate various modes of heat transfer that are present in the large-scale, three different values of the flame heat flux, $\dot{q}''(0)$, were used in the flame spread model as described in Section 5. Case (a) used a flame heat flux equal to 5.2 kW/m^2 (convection only), Case (b) used a heat flux equal

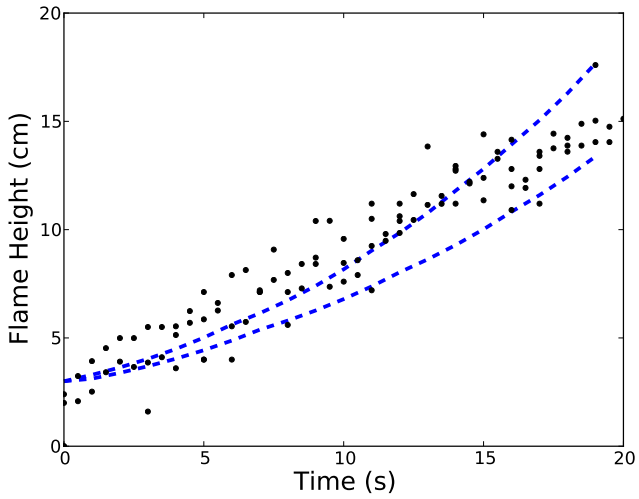

(a) Corrugated cardboard

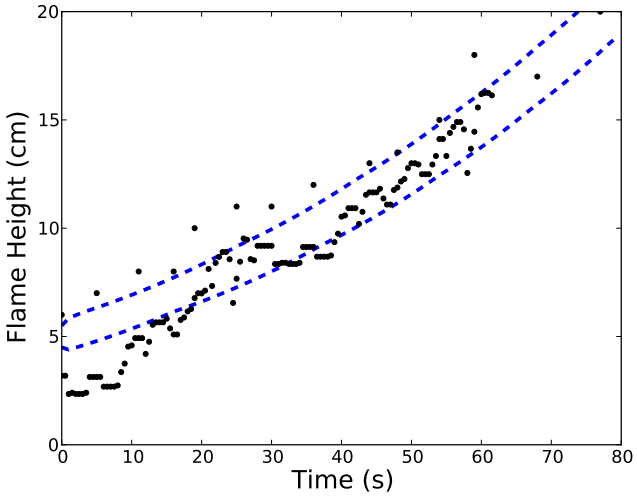

(b) Polystyrene

Figure 10: *Flame heights in the bench-scale tests compared to the predicted flame heights. The points indicate the measured flame heights, and the dashed lines indicate the upper and lower bounds of the predicted flame heights by incorporating the standard deviation of the calculated B-number as follows: (a) Corrugated cardboard:* $B = 1.61$ *and* $B = 1.73$*, (b) Polystyrene:* $B = 1.38$ *and* $B = 1.44$*.*

Figure 11: *A large-scale fire test as the flame spreads up through the flue space between the packed commodity boxes [52].*

to 80 kW/m^2 (radiation heat transfer coefficient), and Case (c) used a heat flux equal to 27 kW/m^2 (radiation flue correlation).

The flame heat flux that resulted in the best in-rack flame height predictions, Case (c), accounts for both convective and radiative heat transfer by using a radiation correlation based on heat transfer between two parallel plates as shown in Eq. 13a. This is the most representative of the fire conditions in the large-scale warehouse fire tests because the fire is ignited in the flue space between the commodity boxes and spreads upwards between the stack of commodity boxes. In this case, radiant energy feedback was occurring between the parallel fuel surfaces as the flames grew larger and increased the flame heat flux and the flame spread rate. The model shows good agreement for the initial stage of fire growth at the large-scale in which the primary fuel is the cardboard packaging of the cartons.

Additionally, Figure 12 includes a comparison to several existing correlations to large-scale, in-rack flame heights and corrugated cardboard flues for comparison. Alvares et al. [8] performed experiments on the impact of separation distance between parallel panels of corrugated cardboard on the in-rack flame height as a function of time and presented a correlation, $x_f = 0.24e^{(1.5/d+0.01)(t-t_0)}$, where d is the separation distance between the panels. This correlation is shown as a dotted line in Figure 12 where the separation distance was fixed as 0.015 m, as was present in the UL tests. Flame heights between solid sheets of cardboard are significantly lower than

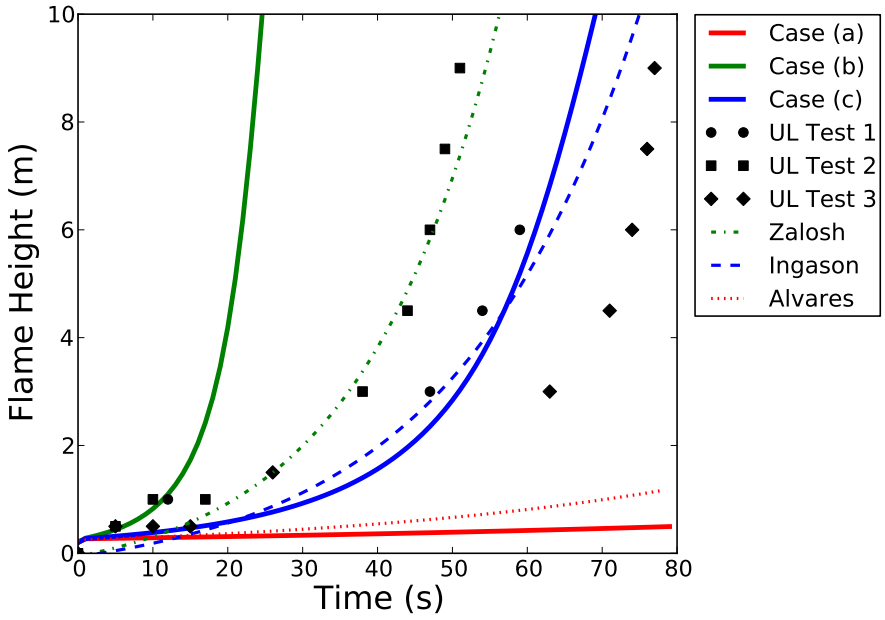

Figure 12: *Observed in-rack flame heights from three large-scale UL experiments (points) are compared to the predicted flame heights (solid lines) using three different heat flux models, which correspond to the following three heat fluxes: a) 5.2 kW/m^2 (convection only), b) 80 kW/m^2 (radiation heat transfer coefficient), and c) 27 kW/m^2 (radiation flue correlation). Additionally, flame height predictions are shown for three existing correlations (Zalosh, Ingason, and Alvares) for comparison, as described in the text.*

rack-storage test data, which may have been caused by different types of cardboard (not specified in Alvares et al.) or the greater oxygen entrainment in the rack-storage configuration due to additional side flues that increased the heat flux in the center flue and, therefore, flame heights and flame spread rates.

Ingason performed reduced-scale to large-scale experiments on multiple-wall corrugated paper cartons in rack-storage configurations and measured in-flue flame heights, which were correlated with flame heights as $x_f = -3.73d + 0.343Q^{2/5}$, where d is the flue space between the racks, and Q is the heat release rate measured by oxygen-consumption calorimetry [10]. While the type of cardboard used in this correlation was different (double tri-wall rather than single 'C' flute cardboard), a very similar correlation was developed by Ingason and de Ris [9], $L_f = 0.315Q^{2/5} - 3.54w$, where the correlation nearly perfectly matches even though it was performed with a gas burner on storage geometries composed of simulated metal. This supports the contention that this correlation is based on geometry, not the fuel, and is still appropriate in this case. To compare this in-rack flame height correlation to the results of this study as a function of time, the heat release rates of full-scale rack-storage experiments have been used in the comparison. Exponential fits to rack-storage data agree best with the present flame height data, and a correlation of heat release rates by Ingason [53] to 4-tier, double tri-wall corrugated board, $Q = 2.266e^{0.102t}$, which is shown as a dashed line in Figure 12.

A range of other experimental correlations are available in Zalosh [13] where polystyrene chips represent the worst-case scenario, and the corresponding flame height is shown as a dash-dot line in Figure 12. The slowest advancing case shown in Zalosh (Figure 5.15), which is Prototype class II and is only 2 tiers high, does not appear in Figure 12. Although the present curves do fall within the range of the observed in-rack flame heights, heat release data for full-scale tests as tall as the UL tests (9.1 m) was not found by the authors in the available literature, which reinforces the need for more universal correlations that do not necessitate new full-scale tests to predict results whenever a parameter is modified. One must remember that these data were derived directly from experimental tests performed at UL, whereas the modification of the Sibulkin and Kim model match the data due to experimental parameters that can be measured at the small scale.

7. Conclusions

In this study, a bench-scale method was used to experimentally determine the average B-number of a given material, and the results from the bench-scale tests were then used to model flame heights in the flue space during a warehouse test with commodity stacked up to a height of 9.1 m (30 ft). The flame spread model that showed the best agreement with the large-scale experimental flame heights (Figure 12) used the flame heat flux that incorporates both convective heat transfer and a correlation for radiative heat transfer between parallel plates.

Therefore, using this bench-scale B-number calculation method, the processes of heat transfer (flow conditions) and mass transfer (B-number) were coupled and expressed independently of one another, which enabled the extrapolation of the mass-loss rates from the bench-scale tests to the early stage of the large-scale warehouse conditions. The B-number was obtained from bench-scale experiments where the flow conditions were mostly laminar and could be controlled to better understand the effects of material properties. Three different flow conditions were used to model heat transfer in the large-scale, and the in-rack flame heights were compared to previous experimental correlations by using large-scale commodity fire test data.

Additionally, because the soot yield (Y_s) is nondimensional, intrinsic to a given material, and can be measured at the bench-scale, it can be a useful parameter to model the radiation effects at the large-scale. As Y_s increases, the radiant feedback from the gas phase combustion to the fuel increases, which results in an increased rate of flame spread. Future work involves more understanding of the physical interaction between multiple material samples to quantify the effects of a mixed commodity on the overall flame spread process.

This method has demonstrated that the B-number can be determined from bench-scale test methods and utilized in flame height predictions that are valid in large-scale fires. In future work, the soot yield (Y_s) can also be determined from bench-scale tests and incorporated into the model. This is important because the flammability of a commodity is coupled with the upward flame spread process, which is the most significant hazard in a warehouse storage fire, and the B-number and soot yield seem to describe the process well for the vertical flue space in the warehouse scenario. A framework has been demonstrated for which the results from bench-scale tests can be used to predict large-scale flame heights of single fuels at the large scale.

If the pyrolysis rate of the fuels is effectively described by the B-number in CFD codes, then the flow conditions for more complex geometries may be more easily resolved, which highlights the potential applications of this work in the future. The B-number and soot yield are fundamentally robust parameters that may be used in the future as means to classify the flammability of a given warehouse commodity, to strengthen the level of confidence in determining the flammability of a commodity, and to increase the effectiveness of warehouse fire protection and suppression applications. Additionally, the results of this study are useful for the application of sprinkler activation and determining the amount of sprinkler suppression that is necessary as a fire grows larger.

8. Acknowledgements

Special thanks is extended to Randall Harris at the WPI Fire Science Laboratory for his assistance with the bench-scale experiments. The authors would like to thank José Torero at the University of Edinburgh and John de Ris at FM Global for their useful discussions and insight regarding this study. Commodity samples and test data were generously donated by David LeBlanc at Tyco International. Corrugated cardboard samples were generously donated by Sam Abbott at Abbot-Action in Canton, MA.

References

[1] NFPA 13: Standard for the Installation of Sprinkler Systems, National Fire Protection Association, 2007.

[2] M.J. Gollner, K.J. Overholt, F.A. Williams, A.S. Rangwala, J. Perricone, Warehouse Commodity Classification from Fundamental Principles. Part I: Commodity & Burning Rates, Fire Safety Journal, Under Review.

[3] J. Harrington, Lessons learned from understanding warehouse fires, Fire Protection Engineering, Winter, 2006.

[4] A. Hamins, K.B. McGrattan, Reduced-scale experiments on the water suppression of a rack-storage commodity fire for calibration of a CFD fire model, NIST Technical Report NISTIR 6439 (1999) 457–468.

[5] G. Grant, D. Drysdale, Numerical modelling of early flame spread in warehouse fires, Fire Safety Journal 24 (3) (1995) 247–278.

[6] K. Saito, J.G. Quintiere, F.A. Williams, Upward turbulent flame spread, Fire Safety Science—Proceedings of the First International Symposium (1985) 75—86.

[7] B. Karlsson, A mathematical model for calculating heat release rate in the room corner test, Fire Safety Journal 20 (1993) 93–113.

[8] N. Alvares, H.K. Hasegawa, K. Hout, A.C. Fernandez-Pello, J. White, Analysis of a run-away high rack storage fire, Fire Safety Science – Proceedings of the Fourth International Symposium (1994) 1–12.

[9] H. Ingason, J. de Ris, Flame heat transfer in storage geometries, Fire Safety Journal 31 (1) (1998) 39–60.

[10] H. Ingason, Plume flow in high rack storages, Fire Safety Journal 36 (5) (2001) 437–457.

[11] J.L. Lee, Stored Commodity Fire Test Program Part I: Fire Products Collector Tests, Prepared for The Society of the Plastics Industry, 1987.

[12] M. Delichatsios, A Scientific Analysis of Stored Plastic Fire Tests, Fire Science and Technology 3 (2) (1983) 73–103.

[13] R. Zalosh, Industrial Fire Protection Engineering, John Wiley and Sons, 2003.

[14] R.D. Spaulding, Evaluation of Polyethylene and Polyethylene Terepthalate Commodities Using the Fire Products Collector, FMRC IJ 0P0J2.RA.

[15] J. de Ris, L. Orloff, Flame heat transfer between parallel panels, Fire Safety Science - Proceedings of the Eighth International Symposium (2005) 1–12.

[16] J. de Ris, G.H. Markstein, L. Orloff, P. Beaulieu, Similarity of turbulent wall fires, Fire Safety Science - Proceedings of the Seventh International Symposium (2003) 259–269.

[17] M. Foley, The use of small scale fire test data for the hazard assessment of bulk materials, Ph.D. thesis, University of Edinburgh (1995).

[18] M. Foley, D. Drysdale, Heat transfer from flames between vertical parallel walls, Fire Safety Journal 24 (1995) 53–73.

[19] D.B. Spalding, Combustion of a Single Droplet and of a Fuel Spray, Selected Combustion Problems, Agard Combustion Colloquium, Butterworths Scientific Publications, London (1954) 340–351.

[20] H. Emmons, The film combustion of liquid fuel, Z. Angew. Math. Mech. (1956) 60–71.

[21] F.J. Kosdon, F.A. Williams, C. Buman, Combustion of vertical cellulosic cylinders in air, Proc. Comb. Inst. 12 (1969) 253–264.

[22] J.S. Kim, J. de Ris, Laminar burning between parallel fuel surfaces, International Journal of Heat and Mass Transfer 17 (1974) 439–451.

[23] R.S. Silver, Application of the Reynolds Analogy to Combustion of Solid Fuels, Nature, London 165 (1950) 75.

[24] T. Chilton, A. Colburn, Mass transfer (absorption) coefficients prediction data-on heat transfer fluid motion, Ind, Industr. Engng Chem 26 (1934) 1183–1187.

[25] V. Raghavan, A.S. Rangwala, J.L. Torero, Laminar flame propagation on a horizontal fuel surface: Verification of classical Emmons solution, Combustion Theory and Modelling 13 (1) (2009) 121–141.

[26] D.B. Spalding, Experiments on the burning and extinction of liquid fuel spheres, Fuel 32 (1953) 169–185.

[27] A.S. Rangwala, S.G. Buckley, J.L. Torero, Analysis of the constant B-number assumption while modeling flame spread, Combustion and Flame 152 (3) (2008) 401–414.

[28] D.J. Holve, R.F. Sawyer, Diffusion controlled combustion of polymers, Proc. Comb. Inst. 15 (1975) 351–361.

[29] K. Annamalai, M. Sibulkin, Flame spread over combustible surfaces for laminar flow systems Part II: Flame heights and fire, Combustion Science and Technology 19 (5) (1979) 185–193.

[30] K. Annamalai, M. Sibulkin, Flame spread over combustible surfaces for laminar flow systems Part I: Excess fuel and heat flux, Combustion Science and Technology 19 (5) (1979) 167–183.

[31] A.S. Rangwala, Flame Spread Analysis using a Variable B-Number, Proc. Fire Safety Sci. 9.

[32] F.A. Williams, Combustion Theory, Perseus Books, 1985.

[33] Y. Pizzo, J.L. Consalvi, B. Porterie, A transient pyrolysis model based on the B-number for gravity-assisted flame spread over thick PMMA slabs, Combustion and Flame 156 (2009) 1856–1859.

[34] Y. Pizzo, J.L. Consalvi, P. Querre, M. Coutin, L. Audouin, B. Porterie, J.L. Torero, Experimental observations on the steady-state burning rate of a vertically oriented PMMA slab, Combustion and Flame 152 (3) (2008) 451–460.

[35] L. Orloff, J. de Ris, G.H. Markstein, Upward turbulent fire spread and burning of fuel surface, Fire and Explosion Research (1974) 1–10.

[36] A.S. Rangwala, S.G. Buckley, J.L. Torero, Upward flame spread on a vertically oriented fuel surface: The effect of finite width, Proc. Comb. Inst. 31 (2) (2007) 2607–2615.

[37] D. Drysdale, An Introduction to Fire Dynamics, Wiley, Chichester; New York, 1999.

[38] P.J. Pagni, T.M. Shih, Excess Pyrolyzate, Proc. Comb. Inst. 16 (1977) 1329–1343.

[39] J.G. Quintiere, Fundamentals of Fire Phenomena, John Wiley, Chichester, 2006.

[40] C.K. Law, F.A. Williams, Kinetics and convection in the combustion of alkane droplets, Combustion and Flame 19 (1972) 393–405.

[41] S. R. Turns, An Introduction to Combustion: Concepts and Applications, McGraw-Hill, New York, 2000.

[42] M. Sibulkin, J. Kim, The Dependence of Flame Propagation on Surface Heat Transfer II: Upward Burning, Combustion Science and Technology (1977) 1–11.

[43] M. Sibulkin, C. Lee, Flame propagation measurements and energy feedback analysis for burning cylinders, Combustion Science and Technology 9 (3) (1974) 137–147.

[44] J. de Ris, Spread of a laminar diffusion flame, Symposium (International) on Combustion 12 (1) (1969) 241 – 252.

[45] R.E. Mark, Handbook of Physical and Mechanical Testing of Paper and Paperboard, Vol. 2, Marcel Dekker, Inc. New York and Basel, 1984.

[46] M. Chaos, M.M. Khan, N. Krishnamoorthy, J. de Ris, S.B. Dorofeev, Evaluation of optimization schemes and determination of solid fuel properties for CFD fire models using bench-scale pyrolysis tests, Proc. Comb. Inst. 33 (2) (2011) 2599–2606.

[47] SFPE Handbook of Fire Protection Engineering, National Fire Protection Association; Society of Fire Protection Engineers, Quincy, MA.; Bethesda, MD, 2002.

[48] Y. Xin, M. Khan, Flammability of combustible materials in reduced oxygen environment, Fire Safety Journal 42 (8) (2007) 536–547.

[49] A.C. Fernandez-Pello, T. Hirano, Controlling mechanisms of flame spread, Combustion Science and Technology 32 (1) (1983) 1–31.

[50] J.P. Holman, Heat Transfer, 6th Edition, New York: McGraw-Hill Book Co., 1986.

[51] K. Overholt, Characterizing the Flammability of Storage Commodities Using an Experimentally Determined B-number, Master's thesis, Worcester Polytechnic Institute (2009).

[52] J. Golinveaux, D. LeBlanc, Is the code right? New warehouse fire test experience, Presentation. 2008 World Safety Conference & Exposition. Las Vegas, NV (June 2008).

[53] H. Ingason, In-rack fire plumes, Fire Safety Science 5 (1997) 333–344.